PHYSICAL REVIEW C **102**, 051301(R) (2020)

Rapid Communications

Doubly-magic character of ^{132}Sn studied via electromagnetic moments of ^{133}Sn

L. V. Rodríguez,[1,2,*] D. L. Balabanski,[3] M. L. Bissell,[4] K. Blaum,[2] B. Cheal,[5] G. De Gregorio,[6,7] J. Ekman,[8] R. F. Garcia Ruiz,[9,†] A. Gargano,[6] G. Georgiev,[10] W. Gins,[11,‡] C. Gorges,[12,§] H. Heylen,[2,9,11] A. Kanellakopoulos,[11] S. Kaufmann,[12] V. Lagaki,[9,13] S. Lechner,[9,14] B. Maaß,[12] S. Malbrunot-Ettenauer,[9] R. Neugart,[15,2] G. Neyens,[9,11] W. Nörtershäuser,[12] S. Sailer,[16] R. Sánchez,[17] S. Schmidt,[12] L. Wehner,[15] C. Wraith,[5] L. Xie,[4] Z. Y. Xu,[11,‖] X. F. Yang,[11,18] and D. T. Yordanov[1,9]

[1]*Institut de Physique Nucléaire, CNRS-IN2P3, Université Paris-Sud, Université Paris-Saclay, 91406 Orsay, France*
[2]*Max-Planck-Institut für Kernphysik, 69117 Heidelberg, Germany*
[3]*ELI-NP, Horia Hulubei National Institute for R&D in Physics and Nuclear Engineering, 077125 Magurele, Romania*
[4]*School of Physics and Astronomy, The University of Manchester, Manchester M13 9PL, United Kingdom*
[5]*Oliver Lodge Laboratory, University of Liverpool, Liverpool L69 7ZE, United Kingdom*
[6]*Istituto Nazionale di Fisica Nucleare, Sezione di Napoli, 80126 Napoli, Italy*
[7]*Dipartimento di Matematica e Fisica, Università degli Studi della Campania "Luigi Vanvitelli", 81100 Caserta, Italy*
[8]*Department of Materials Science and Applied Mathematics, Malmö University, Malmö, Sweden*
[9]*Experimental Physics Department, CERN, 1211 Geneva 23, Switzerland*
[10]*CSNSM, CNRS-IN2P3, Université Paris-Sud, Université Paris-Saclay, 91406 Orsay, France*
[11]*Instituut voor Kern- en Stralingsfysica, KU Leuven, 3001 Leuven, Belgium*
[12]*Institut für Kernphysik, Technische Universität Darmstadt, 64289 Darmstadt, Germany*
[13]*Institut für Physik, Universität Greifswald, 17487 Greifswald, Germany*
[14]*Technische Universität Wien, Karlsplatz 13, 1040 Wien, Austria*
[15]*Institut für Kernchemie, Universität Mainz, 55128 Mainz, Germany*
[16]*Technische Universität München, 80333 Munich, Germany*
[17]*GSI Helmholtzzentrum für Schwerionenforschung GmbH, 64291 Darmstadt, Germany*
[18]*School of Physics, State Key Laboratory of Nuclear Physics and Technology, Peking University, Beijing 100871, China*

(Received 10 August 2020; accepted 20 October 2020; published 9 November 2020)

We report the first measurement of the magnetic dipole and electric quadrupole moment of the exotic nucleus ^{133}Sn by high-resolution laser spectroscopy at ISOLDE/CERN. These, in combination with state-of-the-art shell-model calculations, demonstrate the single-particle character of the ground state of this short-lived isotope and, hence, the doubly-magic character of its immediate neighbor ^{132}Sn. The trend of the electromagnetic moments along the $N = 83$ isotonic chain, now enriched with the values of tin, are discussed on the basis of realistic shell-model calculations.

DOI: 10.1103/PhysRevC.102.051301

In nuclear physics, certain numbers of protons (Z) or neutrons (N), such as 2, 8, 20, 28, 50, 82, and 126, are known as "magic." These numbers endow the nucleus with a special stability analogous to the chemical stability associated with noble gases. Its existence led to the hypothesis that the nucleus contains shells of nucleons that are similar to the shells of electrons in an atom. About 250 species, of approximately 3000 discovered to date, have magic numbers of protons or neutrons, and only ten of them have magic numbers of both. Among this exclusive group, five nuclides are due to their radioactive nature notoriously difficult to access experimentally. However, thanks to state-of-the-art techniques, detailed spectroscopic information can nowadays be obtained for ^{132}Sn (50 protons and 82 neutrons), the heaviest radioactive doubly-magic nucleus.

During the past decade, many experimental studies have aimed to investigate whether ^{132}Sn, eight neutrons away from the heaviest stable tin isotope, retains its doubly-magic character [1–7]. It is, in fact, well recognized, that the single-particle ordering which underlies nuclear shell structure may change in those nuclei with a large N/Z ratio, leading to the disappearance of classic shell gaps and the appearance of new magic numbers. Clear evidence of this phenomenon has been

*liss.vazquez.rodriguez@cern.ch
†Present address: Massachusetts Institute of Technology, Cambridge, Massachusetts, USA.
‡Present address: Department of Physics, University of Jyväskylä, PB 35 (YFL) FIN-40351 Jyväskylä, Finland.
§Present address: Institut für Kernchemie, Universität Mainz, D-55128 Mainz, Germany.
‖Present address: Department of Physics and Astronomy University of Tennessee, 7996, Knoxville Tennessee, USA.

found for light- and medium-mass nuclei. For instance, it has been shown that in ^{42}Si $N = 28$ is no longer a magic number [8], whereas $N = 16$ does appear to be magic in neutron-rich oxygen isotopes [9–11] and the same is suggested for $N = 32$ and 34 in calcium isotopes [12–14] although the doubly-magic nature of ^{52}Ca is challenged by recent laser-spectroscopy work [15]. As for ^{132}Sn, two transfer-reaction experiments have provided leading information through measurements of spectroscopic factors [16] and lifetimes [17] of ground and excited states in ^{133}Sn. Both experiments have shown that, regardless of its large neutron-to-proton ratio, this nucleus can be considered a very robust doubly-magic core. Such a finding is of importance in current nuclear structure research as the persistence of (double-) magicity despite an unbalanced N/Z ratio may shed light into the detailed mechanism causing the unexpected shell evolution in other areas of the nuclear landscape. Furthermore, it validates the choice of ^{132}Sn as a closed core in shell-model calculations, making them a reliable tool to describe this mass region, which is important for the rapid neutron-capture process creating elements in merging neutron stars [18,19].

In this Rapid Communication, we report new evidence of the doubly-magic character of ^{132}Sn through a measurement of the electromagnetic moments of ^{133}Sn using high-resolution collinear laser spectroscopy. The experimental data, in combination with state-of-the-art shell-model calculations, clearly show that ^{132}Sn plays a prominent role as a closed core and can, therefore, be used to describe more complex systems in this region. This is confirmed on higher-mass isotones ($N = 83$) for which experimental moments are found to be well described by theory.

The beam of ^{133}Sn was produced at ISOLDE/CERN. High-energy protons impinging on a tungsten rod generated spallation neutrons, which, in turn, induced fission in a uranium carbide target [20]. Following laser ionization [21], electrostatic acceleration to 40 or 50 keV and mass selection, the ions were injected into a linear Paul trap [22], which provided bunched beams with a temporal width of about 5 μs. Fast ion bunches were released to the collinear laser spectroscopy beam line, postaccelerated and neutralized by charge exchange with sodium vapor [23,24]. A continuous-wave laser beam was collinearly superimposed with the bunched atomic beam. The laser frequency was kept fixed whereas the Doppler-shifted frequency was scanned by varying the potential applied to the charge-exchange cell. The fluorescence emitted from the laser excited atomic beam was imaged by telescopes of aspheric lenses onto four photomultiplier tubes. To suppress background events a time gate corresponding to the laser and atom-bunch interaction time was applied to the photon signal. Details concerning the experimental setup can be found in the review by Neugart *et al.* [25]. A sketch of the collinear laser spectroscopy beamline is given in Ref. [26].

Hyperfine structures were measured in two complementary transitions of the neutral tin atom, shown in Fig. 1. The transition $5p^2\,{}^1S_0 \rightarrow 5p6s\,{}^1P_1$ at 453 nm offers a large quadrupole splitting whereas the transition $5p^2\,{}^3P_0 \rightarrow 5p6s\,{}^3\mathrm{P}_1$ at 286 nm provides high sensitivity to magnetic moments. The laser light was produced by frequency doubling the fundamental light of

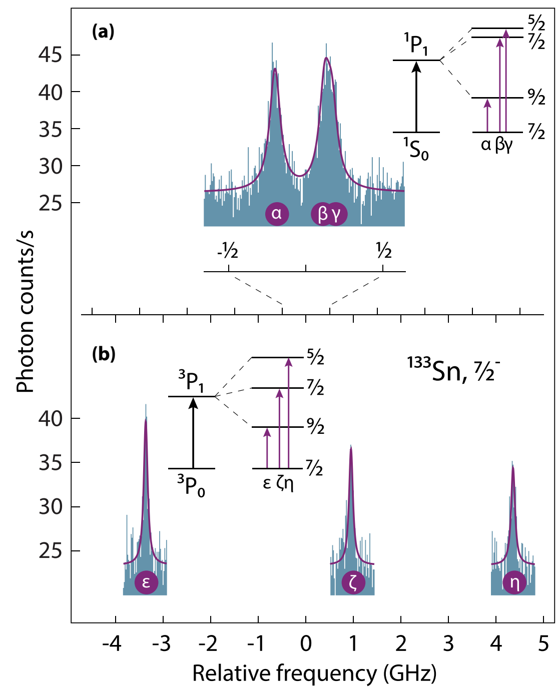

FIG. 1. Hyperfine spectra of ^{133}Sn: (a) in the $5p^2\,{}^1S_0 \rightarrow 5p6s\,{}^1P_1$ and (b) in the $5p^2\,{}^3P_0 \rightarrow 5p6s\,{}^3\mathrm{P}_1$ transitions. The horizontal axis is relative to the fine-structure transition. Solid lines represent a simultaneous fit of the two transitions.

a continuous-wave single-mode ring laser, operated either as titanium sapphire or dye.

Example hyperfine spectra of ^{133}Sn are presented in Fig. 1. Simultaneous analysis of the two transitions was conducted within the ROOT framework [27]. A combined χ^2 was built and minimized using the WrappedMultiTF1 class and the MINUIT2 minimization package. The hyperfine A and B coefficients of the triplet state (${}^3P_1$) and singlet state (${}^1P_1$), respectively, were free parameters of the fit since these exhibit the larger response to the nuclear moments. The resonances were defined by

$$E_F - E_J = \begin{cases} c_1 R_A A({}^3P_1) + c_2 B({}^1P_1) & \text{for } {}^1P_1, \\ c_1 A({}^3P_1) + c_2 R_B B({}^1P_1) & \text{for } {}^3P_1, \end{cases}$$

where c_1 and c_2 are constants that depend on the nuclear, electronic, and total angular momentum quantum numbers [28]. The ratios of hyperfine coupling constants were defined with the aid of additional spectra, obtained in the same experimental run as explained below. $R_A = A({}^1P_1)/A({}^3P_1) = 0.0517(2)$ was determined with high accuracy from simultaneously fitting the $1/2^+$ states, which do not undergo quadrupole splitting in ^{115,117,119}Sn [26]. It was then used as a constraint in the fitting of the spectra of ^{133}Sn and ^{109}Sn also performed simultaneously. The addition of ^{109}Sn in the analysis aided the precision of the extracted $R_\mathrm{B} = B({}^3P_1)/B({}^1P_1) = -0.25(2)$ which was then adopted as a constraint in the analysis of the odd-mass isotopes $^{117-131}$Sn [26].

The line profiles for the fitting were described by a symmetric Voigt function [29]. The linewidth and background level were kept free and independent for each spectrum. The

TABLE I. Electromagnetic moments of the $I = 7/2^-$ ground state of $N = 83$ isotones from this work and from literature. Shell-model calculations using microscopic (Calc-M) as well as empirical (Calc-E) effective operators are included in the table.

	A	Exp.	Ref.	Calc-M	Calc-E
			Magnetic moment (μ_N)		
Sn	133	−1.410(1)	This work	−1.37	−1.34
Te	135	−0.690(50)	[35]	−1.17	−1.13
Xe	137	−0.968(8)	[36]	−1.13	−1.10
Ba	139	−0.973(5)	[37]	−1.11	−1.09
Ce	141	−1.090(40)	[38]	−1.10	−1.09
Nd	143	−1.063(5)	[39]	−1.11	−1.10
Sm	145	−1.123(11)	[41]	−1.12	−1.11
Gd	147	−1.020(90)	[42]	−1.11	−1.11
Dy	149	−1.119(9)	[43]	−1.10	−1.10
			Quadrupole moment (b)		
Sn	133	−0.145(4)(10)[a]	This work	−0.13	−0.16
Te	135	+0.290(90)	[35]	−0.30	−0.33
Xe	137	−0.480(20)	[36]	−0.36	−0.39
Ba	139	−0.573(13)	[37]	−0.39	−0.43
Ce	141			−0.43	−0.51
Nd	143	−0.610(21)	[40]	−0.46	−0.50
Sm	145	−0.600(70)	[41]	−0.47	−0.51
Gd	147			−0.48	−0.52
Dy	149	−0.620(50)	[43]	−0.51	−0.56

[a]Statistical uncertainty is shown in a first set of parentheses and systematic uncertainty due to the electric-field gradient is shown in a second set of parentheses.

relative peak intensities were fixed to the Racah coefficients [30] for the $^1P_1$ state and were free parameters for the fully resolved $^3P_1$ state.

The effect of the hyperfine anomaly in ^{133}Sn due to the extended distribution of the magnetization over the nuclear volume [31] and the extended nuclear charge distribution [32], was estimated using a developer version of the General Relativistic Atomic Structure Package GRASP2K [33]. The two-parameter Fermi model was used as the charge distribution and the magnetic distribution was approximated with the square of the harmonic-oscillator wave function of the last uncoupled neutron with $\hbar/(m\omega) = A^{1/3}$. The resulting hyperfine anomaly,

$$^{119}\Delta^{133} = \frac{A^{119}}{A^{133}}\frac{g^{133}}{g^{119}} - 1 = 0.075\% \qquad (1)$$

is smaller than the uncertainty of the magnetic moment. It was, therefore, neglected during the fit and further treated as a contribution to the experimental error.

By linking two independent measurements of the hyperfine structure in two $J{:}\,0 \rightarrow 1$ transitions we were able to confirm the spin $I = 7/2$ for the ground state. The electromagnetic moments, presented in Table I, were evaluated from the measured hyperfine parameters $A(^3P_1) = -965.2(5)$ and $B(^1P_1) = -102(3)$ MHz, through the following expressions:

$$A\frac{I}{\mu} = \text{const} = 2396.6(7)\ \text{MHz}/\mu_N, \qquad (2)$$

$$\frac{B}{Q} = \text{const} = 706(50)\ \text{MHz/b}. \qquad (3)$$

The constants above are taken from Ref. [26] and represent the average magnetic field per unit angular momentum and the electric field gradient generated by the electron cloud at the position of the nucleus, respectively.

This measurement completes the sequence of ground-state moments of $N = 83$ isotones from tin to dysprosium as shown in Fig. 2. In the extreme single-particle shell model, the $7/2^-$ ground state of all these isotones are expected to be dominated by configurations with one valence neutron in the $1f_{7/2}$ orbital which can be considered to be almost entirely responsible for the magnetic and quadrupole moment of the nucleus. Consistent with the expectation for a doubly-magic-plus-one-neutron nucleus, both the magnetic and the quadrupole moment of ^{133}Sn are indeed very close to the single-particle estimates for a single neutron in the $1f_{7/2}$ orbital [34], indicated by the straight dotted lines in Fig. 2. On the other hand, for the higher-mass $N = 83$ isotones with an open proton shell, the single-particle shell model is a too crude approximation and the moments deviate from the dotted lines. These observations point to the single-particle character of ^{133}Sn and, hence, confirm the robustness of the ^{132}Sn core. In the following paragraphs, these qualitative findings will be supported by realistic shell model calculations. Note that the case of ^{135}Te does not follow the general trend of the other isotones and will be discussed at the end of this section.

The experimental magnetic dipole and electric quadrupole moments shown in Fig. 2 are also summarized in Table I and compared with theoretical results obtained by performing a realistic shell-model calculation. An effective Hamiltonian was derived from the high-precision CD-Bonn NN potential

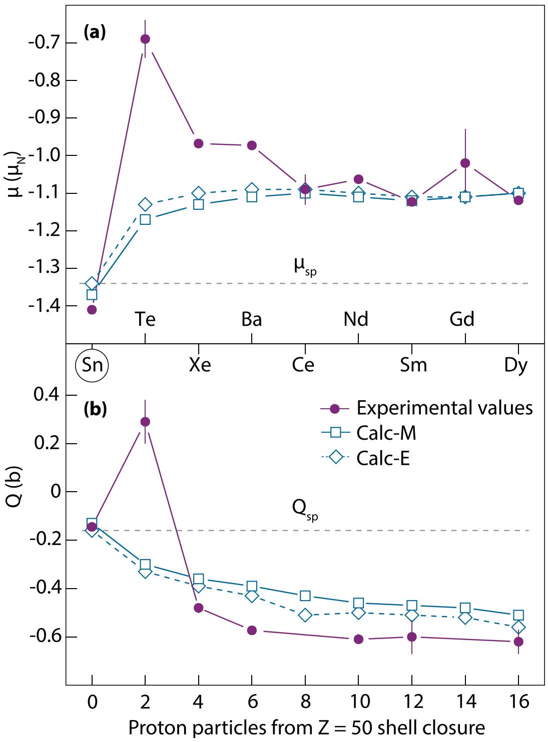

FIG. 2. Magnetic and quadrupole moments (dots) of the $I = 7/2^-$ ground state of $N = 83$ isotones with even Z up to $Z = 66$ compared with shell-model calculations using microscopic (squares) and empirical (diamonds) effective operators. Gray dotted lines represent the effective single-particle estimates for a single neutron in the $1f_{7/2}$ orbital. These single-particle values were obtained by using standard prescriptions for the effective neutron charge and the effective neutron spin gyromagnetic factors, namely, $e(\nu) = 0.7e$ and $g_s(\nu) = 0.7g_s^{\rm free}(\nu)$, a choice supported by the microscopic calculations presented in this work.

[44] renormalized by means of the $V_{\text{low-k}}$ approach [45] with the addition of the Coulomb term for the proton-proton interaction. This Hamiltonian has already been adopted in several previous studies of neutron-rich nuclei beyond ^{132}Sn [46].

The doubly-magic ^{132}Sn was considered as a core and all the neutron orbits of the 82–126 shell ($0h_{9/2}$, $1f_{7/2}$, $1f_{5/2}$, $2p_{3/2}$, $2p_{1/2}$, $0i_{13/2}$) and all the proton orbits of the 50–82 shell ($0g_{7/2}$, $1d_{5/2}$, $1d_{3/2}$, $2s_{1/2}$, $0h_{11/2}$) were included in the model space. The two-body matrix elements of the effective shell-model Hamiltonian for the chosen model space were derived using the $\hat{Q}$ box folded-diagram approach [47,48], including in the perturbative diagrammatic expansion of the $\hat{Q}$ box one and two-body diagrams up to second order in the interaction. The single-proton and single-neutron energies appearing in the one-body term of the Hamiltonian were taken where possible from experiment, namely, from the level schemes of ^{133}Sb and ^{133}Sn [49]. The proton $2s_{1/2}$ and neutron $0i_{13/2}$ energies, which were not available, have been determined by reproducing the experimental energy of the 2150-keV $1/2^+$ state in ^{137}Cs and of the 2423-keV 10^+ state in ^{134}Sb, respectively.

The electromagnetic properties are calculated by employing microscopic (Calc-M) as well as empirical (Calc-E) effective operators. A standard prescription is adopted for the empirical $M1$ operator, namely, the spin gyromagnetic factors for both protons and neutrons are quenched to 70% of their bare values, whereas the orbital ones are not modified [50]. The empirical $E2$ operators are obtained by choosing an effective proton charge of $e_p = 1.7e$ and an effective neutron charge of $e_n = 0.7e$, which reproduce the experimental $B(E2; 0_1^+ \to 2_1^+)$ values in ^{134}Te and ^{134}Sn [49]. On the other hand, the single-particle matrix elements of the effective microscopic $M1$ and $E2$ operators are calculated within the same framework of the shell-model Hamiltonian by employing the Suzuki-Okamoto formalism [51], that is an extension of the $\hat{Q}$ box-plus-folded diagram method for transition operators. Details on this procedure can be found in Ref. [52]. Shell-model calculations have been carried out using the shell-model code KSHELL [53]. Within the adopted model space, with ^{132}Sn as a core, ^{133}Sn is a one-valence system. Therefore, the results for ^{133}Sn from Calc-E coincide with the single-particle estimates shown in Fig. 2.

The values predicted by both calculations are very close to each other. In fact, the renormalization of the bare one-body matrix elements of the $M1$ and $E2$ operators derived within the perturbative approach are consistent with the corrections introduced by using empirical effective charges and gyromagnetic factors. In particular, from Table I we see that the empirical and microscopic $M1/E2$ operator produces about the same diagonal single-particle matrix element for the $1f_{7/2}$ neutron orbit, that is very close to the experimental value of ^{133}Sn. From a quantitative point of view the predictions of both calculations are in good agreement with the experimental data also for the higher-mass isotones, except for ^{135}Te which will be discussed at the end of the paper. In fact, discrepancies for magnetic moments are less than $0.1\mu_N$ in most of the cases, reaching the maximum value of $0.13\mu_N$ in ^{137}Xe, whereas for the electric moments the largest difference between theory and experiment is 0.14b in ^{139}Ba.

It is worth noting that, starting from ^{137}Xe with four valence protons, the observed overall trends of the magnetic dipole and electric quadrupole moments are well reproduced by the theory as shown in Fig. 2. The behavior of the two curves essentially reflects the effects of valence protons, which give a positive contribution to the magnetic moments and a negative contribution to the quadrupole moments, determining their respective decrease and increase in magnitude as compared to the values of ^{133}Sn. The ground state of a $N = 83$ nucleus can be written in terms of a neutron coupled to the $N = 82$ neighbor. Since protons coupled to a spin 0 do not contribute to the magnetic or quadrupole moment, these proton contributions arise mainly due to $\pi 2_1^+ \otimes \nu f_{7/2}$ configurations as shown by our calculations. Actually, we find that, whereas the $\pi 0_{\rm gs}^+ \otimes \nu f_{7/2}$ component accounts for ≈85% of the calculated wave functions of the $N = 83$ ground states, a non-negligible percentage -ranging from 5 to 6%-, comes also from the $\pi 2_1^+ \otimes \nu f_{7/2}$ component. This 5 to 6% contribution in the wave function, indeed, results in an increase in magnetic moment and the amount depends on the magnetic moments of the yrast 2^+ state in the $N = 82$ isotones. By using the experimental 2^+ magnetic moments, which are known from ^{136}Xe up to ^{144}Sm and range in value between +1.5 and

$+1.9\mu_{\mathrm{N}}$ [49], the magnetic moments of the $N = 83$ ground states are reproduced quite well in a simple two-level mixing calculation, which confirms the reliability of our predictions for their wave functions. Similar considerations are not possible, unfortunately, for the electric quadrupole moments. In fact, the required quadrupole moments of the yrast 2^+ state in the $N = 82$ isotones have been measured only for ^{138}Ba and the sign of the $\langle \pi 2_1^+ | E2 | \pi 0_{\mathrm{gs}}^+ \rangle$ matrix element, which also comes into play, is unknown.

In concluding, it is worth underlining that, although both microscopic and empirical calculations give a quite reasonable account of the experimental data, they are not able to reproduce the observed staggering for the magnetic moments, which may be related to changes in the structure of the proton wave functions not accounted by the adopted theoretical approach. Furthermore, the location of both theoretical curves for the quadrupole moment, which is slightly above the experimental one by 0.1b, suggests the need for a further small renormalization of the proton charge.

Regarding ^{135}Te, we observe that both experimental magnetic and quadrupole moments show a strong deviation from the experimental systematics and the calculated values. As suggested by the above discussion, the disagreement between theory and experiment implies that our calculations for the ground-state wave function of ^{135}Te underestimate the percentage of components including excited states of ^{134}Te. This conclusion, however, is not in line with the results of higher-mass $N = 83$ isotones. On this basis, a remeasurement of the electromagnetic moments of ^{135}Te is required in order to clarify the true structure of its ground state.

We have presented the first measurement of the magnetic dipole and electric quadrupole moment of ^{133}Sn by high-resolution laser spectroscopy. The obtained electromagnetic moments approach the single-particle estimates for a single neutron in the $1f_{7/2}$ orbital suggesting a single-particle behavior on top of a closed ^{132}Sn core. Both magnetic and quadrupole moments are very well reproduced by theory, which gives also a good description of the moments of the higher-mass $N = 83$ isotones. We have also shown that the trend along the isotonic chain can be explained in simple terms by decomposing the ground-state wave functions of the $N = 83$ isotones as an $1f_{7/2}$ neutron coupled to the yrast 0^+ and 2^+ states of the $N = 82$ neighbors. The perturbative approach used to derive the microscopic effective $M1$ and $E2$ operators, which does not need the introduction of adjustable parameters, induces the correct renormalizations.

This work has been supported by the Max-Planck Society, the German Federal Ministry for Education and Research under Contract No. 05P18RDCIA, the Helmholtz International Center for FAIR within the LOEWE Program by the State of Hesse, the Belgian IAP Project No. P7/12, the FWO-Vlaanderen, GOA 15/010 from KU Leuven, the European Union seventh framework through ENSAR under Contract No. 262010, the Science and Technology Facilities Council (Grants No. ST/P004423/1 and No. ST/P004598/1), and D.L.B. acknowledges support from the EU Development Fund and Competitiveness Operational Program for the ELI-NP Project Phase II (Project No. 1/07.07.2016, COP, ID1334). We acknowledge the CINECA Award under the ISCRA initiative for the availability of high-performance computing resources and support.

[1] P. Bhattacharyya, P. J. Daly, C. T. Zhang, Z. W. Grabowski, S. K. Saha, R. Broda, B. Fornal, I. Ahmad, D. Seweryniak, I. Wiedenhöver, M. P. Carpenter, R. V. F. Janssens, T. L. Khoo, T. Lauritsen, C. J. Lister, P. Reiter, and J. Blomqvist, Magic Nucleus ^{132}Sn and Its One-Neutron-Hole Neighbor ^{131}Sn, Phys. Rev. Lett. **87**, 062502 (2001).

[2] M. Dworschak, G. Audi, K. Blaum, P. Delahaye, S. George, U. Hager, F. Herfurth, A. Herlert, A. Kellerbauer, H.-J. Kluge, D. Lunney, L. Schweikhard, and C. Yazidjian, Restoration of the $N = 82$ Shell Gap from Direct Mass Measurements of ^{132,134}Sn, Phys. Rev. Lett. **100**, 072501 (2008).

[3] J. M. Allmond, D. C. Radford, C. Baktash, J. C. Batchelder, A. Galindo-Uribarri, C. J. Gross, P. A. Hausladen, K. Lagergren, Y. Larochelle, E. Padilla-Rodal, and C.-H. Yu, Coulomb excitation of ^{124,126,128}Sn, Phys. Rev. C **84**, 061303(R) (2011).

[4] J. Hakala, J. Dobaczewski, D. Gorelov, T. Eronen, A. Jokinen, A. Kankainen, V. S. Kolhinen, M. Kortelainen, I. D. Moore, H. Penttilä, S. Rinta-Antila, J. Rissanen, A. Saastamoinen, V. Sonnenschein, and J. Äystö, Precision Mass Measurements beyond ^{132}Sn: Anomalous Behavior of Odd-Even Staggering of Binding Energies, Phys. Rev. Lett. **109**, 032501 (2012).

[5] A. E. Stuchbery, J. M. Allmond, A. Galindo-Uribarri, E. Padilla-Rodal, D. C. Radford, N. J. Stone, J. C. Batchelder, J. R. Beene, N. Benczer-Koller, C. R. Bingham, M. E. Howard, G. J. Kumbartzki, J. F. Liang, B. Manning, D. W. Stracener, and C.-H. Yu, Electromagnetic properties of the 2_1^+ state in ^{134}Te: Influence of core excitation on single-particle orbits beyond ^{132}Sn, Phys. Rev. C **88**, 051304(R) (2013).

[6] J. Van Schelt, D. Lascar, G. Savard, J. A. Clark, P. F. Bertone, S. Caldwell, A. Chaudhuri, A. F. Levand, G. Li, G. E. Morgan, R. Orford, R. E. Segel, K. S. Sharma, and M. G. Sternberg, First Results from the CARIBU Facility: Mass Measurements on the r-Process Path, Phys. Rev. Lett. **111**, 061102 (2013).

[7] D. Rosiak *et al.*, Enhanced Quadrupole and Octupole Strength in Doubly Magic ^{132}Sn, Phys. Rev. Lett. **121**, 252501 (2018).

[8] B. Bastin *et al.*, Collapse of the $N = 28$ Shell Closure in ^{42}Si, Phys. Rev. Lett. **99**, 022503 (2007).

[9] A. Ozawa, T. Kobayashi, T. Suzuki, K. Yoshida, and I. Tanihata, New Magic Number, $N = 16$, Near the Neutron Drip Line, Phys. Rev. Lett. **84**, 5493 (2000).

[10] M. Stanoiu *et al.*, $N = 14$ and 16 shell gaps in neutron-rich oxygen isotopes, Phys. Rev. C **69**, 034312 (2004).

[11] B. Alex Brown and W. A. Richter, Magic numbers in the neutron-rich oxygen isotopes, Phys. Rev. C **72**, 057301 (2005).

[12] H. L. Crawford, R. V. F. Janssens, P. F. Mantica, J. S. Berryman *et al.*, β decay and isomeric properties of neutron-rich Ca and Sc isotopes, Phys. Rev. C **82**, 014311 (2010).

[13] F. Wienholtz, D. Beck, K. Blaum *et al.*, Masses of exotic calcium isotopes pin down nuclear forces, Nature (London) **498**, 346 (2013).
[14] D. Steppenbeck, S. Takeuchi, N. Aoi *et al.*, Evidence for a new nuclear magic number from the level structure of ^{54}Ca, Nature (London) **502**, 207 (2013).
[15] R. Garcia Ruiz, M. Bissell, K. Blaum *et al.*, Unexpectedly large charge radii of neutron-rich calcium isotopes, Nat. Phys. **12**, 594 (2016).
[16] K. Jones, A. Adekola, D. Bardayan *et al.*, The magic nature of ^{132}Sn explored through the single-particle states of ^{133}Sn, Nature (London) **465**, 454 (2010).
[17] J. M. Allmond *et al.*, Double-Magic Nature of ^{132}Sn and ^{208}Pb through Lifetime and Cross-Section Measurements, Phys. Rev. Lett. **112**, 172701 (2014).
[18] J. J. Cowan, F.-K. Thielemann, and J. W. Truran, The R-process and nucleochronology, Phys. Rep. **208**, 267 (1991).
[19] K.-L. Kratz, B. Pfeiffer, O. Arndt *et al.*, r-process isotopes in the ^{132}Sn region, Eur. Phys. J. A **25**, 633 (2005).
[20] R. Catherall, J. Lettry, S. Gilardoni, and U. Köster, Radioactive ion beams produced by neutron-induced fission at ISOLDE, Nucl. Instrum. Methods Phys. Res., Sect. B **204**, 235(2003).
[21] V. Fedosseev *et al.*, Ion beam production and study of radioactive isotopes with the laser ion source at ISOLDE, J. Phys. G: Nucl. Part. Phys. **44**, 084006 (2017).
[22] E. Mané, J. Billowes, K. Blaum *et al.*, An ion cooler-buncher for high-sensitivity collinear laser spectroscopy at ISOLDE, Eur. Phys. J. A **42**, 503 (2009).
[23] A. Mueller *et al.*, Spins, moments and charge radii of barium isotopes in the range $^{122-146}$Ba determined by collinear fast-beam laser spectroscopy, Nucl. Phys. A **403**, 234 (1983).
[24] A. Klose *et al.*, Tests of atomic charge-exchange cells for collinear laser spectroscopy, Nucl. Instrum. Methods Phys. Res., Sect. A **678**, 114 (2012).
[25] R. Neugart *et al.*, Collinear laser spectroscopy at ISOLDE: new methods and highlights, J. Phys. G: Nucl. Part. Phys. **44**, 064002 (2017).
[26] D. T. Yordanov, L. V. Rodríguez, D. L. Balabanski *et al.*, Structural trends in atomic nuclei from laser spectroscopy of tin, Commun. Phys. **3**, 107 (2020).
[27] R. Brun and F. Rademakers, ROOT–An object oriented data analysis framework, Nucl. Instrum. Methods Phys. Res., Sect. A **389**, 81 (1997).
[28] H. Kopfermann, *Nuclear Moments* (Academic Press, New York, 1958).
[29] T. Ida, M. Ando, and H. Toraya, Extended pseudo-voigt function for approximating the voigt profile, J. Appl. Cryst. **33**, 1311 (2000).
[30] P. C. Magnante and H. H. Stroke, Isotope shift between ^{209}Bi and 6.3-day ^{206}Bi, J. Opt. Soc. Am. **59**, 836 (1969).
[31] A. Bohr and V. F. Weisskopf, The influence of nuclear structure on the hyperfine structure of heavy elements, Phys. Rev. **77**, 94 (1950).
[32] J. E. Rosenthal and G. Breit, The Isotope Shift in Hyperfine Structure, Phys. Rev. **41**, 459 (1932).
[33] P. Jönsson, G. Gaigalas, J. Bieroń, C. Froese Fischer, and I. P. Grant, New version: Grasp2K relativistic atomic structure package, Comput. Phys. Commun. **184**, 2197 (2013).
[34] G. Neyens, Nuclear magnetic and quadrupole moments for nuclear structure research on exotic nuclei, Rep. Prog. Phys. **66**, 633 (2003).
[35] R. Sifi, F. Le Blanc, N. Barré *et al.*, Laser spectroscopy measurements of neutron-rich tellurium isotopes by COMPLIS, Hyp. Interact. **171**, 173 (2006).
[36] W. Borchers, E. Arnold, W. Neu, R. Neugart, K. Wendt, and G. Ulm, Xenon isotopes far from stability studied by collisional ionization laser spectroscopy, Phys. Lett. B **216**, 7 (1989).
[37] K. Wendt, S. A. Ahmad, C. Ekström *et al.*, Hyperfine structure and isotope shift of the neutron-rich barium isotopes $^{139-146}$Ba and ^{148}Ba, Z. Phys. A **329**, 407 (1988).
[38] W. van Rijswijk, F. G. van den Berg, W. R. Joosten *et al.*, Hyperfine interaction of Ce and La in 3-d ferromagnets, Hyp. Interact. **15**, 325 (1983).
[39] K. F. Smith and P. J. Unsworth, The hyperfine structure of ^{167}Er and magnetic moments of ^{143,145}Nd and ^{167}Er by atomic beam triple magnetic resonance, Proc. Phys. Soc. **86**, 1249 (1965).
[40] P. Aufmuth, A. Bernard, M. Deckwer *et al.*, Hyperfine structure in the configurations $4f^4 6s^2$ and $4f^4 5d6s$ of Nd I, Z. Phys. D **23**, 19 (1992).
[41] J. G. England *et al.*, Isotope shifts and hyperfine splitting in $^{144-154}$Sm I, J. Phys. G: Nucl. Part. Phys. **16**, 105 (1990).
[42] T. I. Kracíková, S. Davaa and M. Finger, Magnetic dipole moments of the ^{147,149}Gd ground states, Hyp. Interact. **34**, 69 (1987).
[43] E. W. Otten, in *Treatise on Heavy Ion Science*, Nuclei Far From Stability, edited by D. A. Bromley (Springer, Boston, 1989), Vol. 8.
[44] R. Machleidt, High-precision, charge-dependent Bonn nucleon-nucleon potential, Phys. Rev. C **63**, 024001 (2001).
[45] S. Bogner, T. T. S. Kuo, L. Coraggio, A. Covello, and N. Itaco, Low momentum nucleon-nucleon potential and shell model effective interactions, Phys. Rev. C **65**, 051301(R) (2002).
[46] B. F. Bayman, A. Covello, A. Gargano, P. Guazzoni, and L. Zetta, Two-neutron transfer in Sn isotopes beyond the $N = 82$ shell closure, Phys. Rev. C **90**, 044322 (2014), and references therein.
[47] L. Coraggio, A. Covello, A. Gargano, N. Itaco, and T. T. S. Kuo, Shell-model calculations and realistic effective interactions, Prog. Part. Nucl. Phys. **62**, 135 (2009).
[48] L. Coraggio, A. Covello, A. Gargano *et al.*, Effective shell-model hamiltonians from realistic nucleon-nucleon potentials within a perturbative approach, Ann. Phys. (NY) **327**, 2125 (2012).
[49] Data extracted using the NNDC On-line Data Service from the ENSDF database.
[50] M. Danchev, G. Rainovski, N. Pietralla, A. Gargano, A. Covello, C. Baktash, J. R. Beene, C. R. Bingham, A. Galindo-Uribarri, K. A. Gladnishki, C. J. Gross, V. Yu. Ponomarev, D. C. Radford, L. L. Riedinger, M. Scheck, A. E. Stuchbery, J. Wambach, C.-H. Yu, and N. V. Zamfir, One-phonon isovector $2^+_{1,\mathrm{MS}}$ state in the neutron-rich nucleus ^{132}Te, Phys. Rev. C **84**, 061306(R) (2011).
[51] K. Suzuki and R. Okamoto, Effective operators in time-independent approach, Prog. Theor. Phys. **93**, 905 (1995).
[52] L. Coraggio, L. De Angelis, T. Fukui, A. Gargano, N. Itaco, and F. Nowacki, Renormalization of the Gamow-Teller operator within the realistic shell model, Phys. Rev. C **100**, 014316 (2019).
[53] N. Shimizu, T. Mizusaki, T. Utsuno, and Y. Tsunoda, Thick-restart block Lanczos method for large-scale shell-model calculations, Comput. Phys. Commun. **244**, 372 (2019).